ACS APPLIED MATERIALS & INTERFACES

www.acsami.org

Research Article

Combining ReaxFF Simulations and Experiments to Evaluate the Structure–Property Characteristics of Polymeric Binders in Si-Based Li-Ion Batteries

Manav Bhati,[#] Quan Anh Nguyen,[#] Sibani Lisa Biswal, and Thomas P. Senftle*

Cite This: *ACS Appl. Mater. Interfaces* 2021, 13, 41956–41967

Read Online

ACCESS | Metrics & More | Article Recommendations | Supporting Information

ABSTRACT: High energy capacity silicon (Si) anodes in Li-ion batteries incorporate polymeric binders to improve cycle life, which is otherwise limited by large volume and stress fluctuations during charging/discharging cycles. Several properties of the polymeric binder play a role in achieving optimal battery performance, including interfacial adhesion strength, mechanical elasticity, and lithium-ion conduction rate. In this work, we utilize atomistic simulations with the ReaxFF force field and complementary experiments to investigate how these properties dictate the performance of Si/binder anodes. We study three C/N/H-based polymer binders with varying structures (pyrolyzed polyacrylonitrile (PPAN), polyacrylonitrile (PAN), and polyaniline (PANI)) to determine how the structure–property characteristics of the binder affect performance. The Si/binder adhesion analysis reveals some counter-intuitive results: although an individual PANI chain has a stronger affinity to Si compared to PPAN, the PANI bulk binds weaker to the Si surface. Interfacial structural analyses from simulations of the bulk phase show that PANI chains have poor stacking at the interface, while PPAN chains exhibit dense and highly ordered stacking behavior, leading to stronger adhesion. PPAN also has a lower Young's modulus compared to PANI and PAN owing to its ordered and less entangled bulk structure. This added elasticity better accommodates volume changes associated with cycling, making it a more suitable candidate for Si anodes. Finally, both simulations and experimental measurements of Li-ion diffusion rates show higher Li mobility through PPAN than PAN and PANI because the ordered stacking of PPAN chains creates channels that are favorable for Li diffusion to the Si surface. Galvanostatic charge–discharge cycling experiments show that PPAN is indeed a highly promising binder for Si anodes in Li-ion batteries, retaining a capacity of ~1400 mAh g^{-1} for 150 cycles. This work demonstrates that the orientation and structure of the polymer at and near the interface are essential for optimizing binder performance as well as showcases the initial steps for binder evaluation, selection, and application for electrodes in Li-ion batteries.

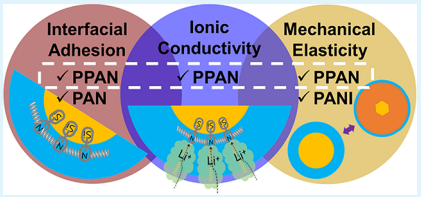

KEYWORDS: *lithium-ion batteries, silicon–binder interaction, reactive force field simulations, structure–property relationship, interfacial adhesion, mechanical elasticity, ion-diffusion channel*

1. INTRODUCTION

The high theoretical lithium (Li) storage capacity of silicon (Si) in a Li-ion battery (3579 mAh g^{-1})[1] gives it an advantage as an anode over its competitors, especially commercial graphite anodes (372 mAh g^{-1}).[2] However, poor cycling performance and short cycle life resulting from large lithiation-induced volume fluctuations in Si anodes (~300%)[3] prevent their commercial adoption. Among several strategies that have been implemented,[4−15] the one that seems promising from the perspective of economy and scalability is that of embedding Si particles in a binder or an elastic organic polymer matrix.[16−21] A binder needs to meet several multifunctional design constraints to be suitable for application in high-capacity Si anodes, and it is challenging to engineer binders that simultaneously meet all selection criteria.[22−26] In this work, we analyze multifunctional structure–property relations of binders using a combination of atomistic simulations and experiments with the goal of identifying the key binder characteristics responsible for improved performance in Si anodes. We compare pyrolyzed polyacrylonitrile (PPAN), chosen because it is a binder for Si with known good performance,[10,16,27−29] to two other C/N/H-based polymers, polyacrylonitrile[30,31] (PAN) and polyaniline[21,32] (PANI), that do not perform as well with Si. The underlying reason for this performance difference is not well understood, as the binders have similar composition. This motivates the atomistic-level study reported here so that we can understand how polymer properties are related to performance. This then will guide effort to engineering binders with optimal structural properties to enhance anode performance.

As laid out in various literature reviews,[22−26] important properties required in a battery binder are (1) strong interfacial

Received: May 7, 2021
Accepted: August 16, 2021
Published: August 25, 2021

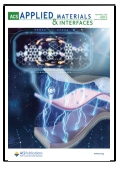

https://doi.org/10.1021/acsami.1c08484
ACS Appl. Mater. Interfaces 2021, 13, 41956–41967

adhesion, (2) high mechanical elasticity, (3) fast ion conduction, (4) fast electron conduction, and (5) prolonged chemical stability, as summarized in Figure 1. First, a strong

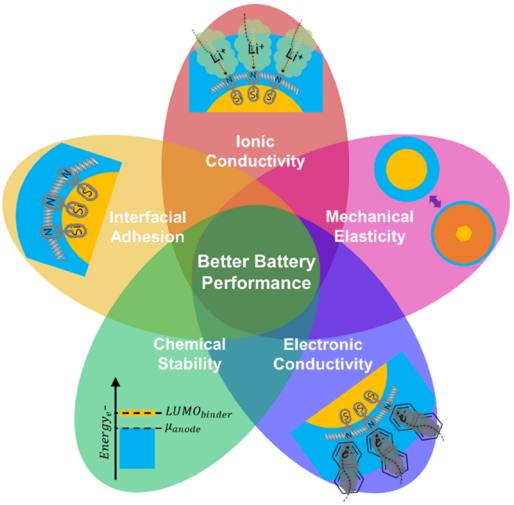

Figure 1. Schematic of key properties of binders for application in battery anodes.

interfacial adhesion between Si and the binder is necessary to maintain the uniformity, continuity, and conductivity of the composite anode. A weakly adhering binder results in Si particles losing contact with the conductive matrix or agglomerating with other Si particles, forming large clusters, which leads to reduced active material and Li capacity. Second, the mechanical elasticity alleviates compressive stress on the binder during the expansion of Si upon lithiation.[33] An elastic binder allows for more lithiation, whereas a stiffer binder constrains Si expansion and causes self-delithiation or lithium retardation.[34,35] Third, binders with high Li-ion conduction are essential, especially for high-power applications, to achieve fast kinetics and improved energy efficiencies. Appropriate ion-diffusion channels in binders play a crucial role in improving ion-conduction.[36] Similarly, an ideal binder matrix also needs to have the capacity to conduct electrons, facilitating charge transport between the Si particles and the current collector. This usually requires the addition of carbon black into the binder matrix in the case of nonconductive polymers, but the use of electronically conductive binders can obviate the need for such an additive, potentially increasing the active material content and creating more efficient pathways for electron transport within the electrode matrix.[23] Finally, any functional binder must be chemically stable in the electrolyte solution (i.e., mostly a mixture of carbonate solvents) as well as resistant to deleterious electrochemical reactions at the electrode (i.e., resistant to reduction and decomposition at the Si anode).[23]

Atomistic simulations can help not only in evaluating these binder properties but also in elucidating the microscopic structural features that are responsible for modulating these properties.[37,38] Such insights are necessary for design efforts seeking to tune each characteristic by engineering the binder's physicochemical features.[37,38,22] Toward this end, reactive molecular dynamics (MD) simulations are most suitable for investigating interfaces separating dissimilar phases, such as the organic binder and inorganic Si, as they allow bonds to form and break during the simulation. Several studies based on reactive MD simulations have previously used ReaxFF force fields to investigate battery materials,[39−41] polymers,[42−44] and interfaces in composite materials.[45−47] We have previously developed a ReaxFF Si/C/N/H force field to understand the interfacial interactions of C/N/H-based polymers with Si surfaces.[48]

In this work, we use ReaxFF simulations and experiments to compare the performance of three widely used C/N/H-based polymer binders in Si composite anodes: PPAN, PAN, and PANI. In terms of chemical stability, all three polymers have demonstrated good compatibility with Si-based battery applications in the literature.[23,25] The electronic conductivity of PAN must be enhanced either by the addition of carbon black or by conversion into its conjugated form (i.e., PPAN) that is highly conductive owing to the presence of sp^2 π-bonding in the structure after heat treatment under an inert atmosphere.[27−29] According to the literature, the pyrolysis of PAN can increase its electronic conductivity by several orders of magnitude, from 10^{-6} to 10^{-1} S cm^{-1}.[49−51] Although the effect of PPAN's 3D conducting network cannot be easily augmented by the addition of carbon black into PAN, we have found that, at 10% carbon additive, Si/PAN electrodes demonstrate a lower resistivity than of Si/PPAN electrodes. Further discussion on this topic can be found in the Supporting Information. As for polyaniline (PANI), its emeraldine form is also electronically conductive upon doping with acid.[52] PANI's electronic conductivity can sharply increase from 10^{-9}−10^{-8} S cm^{-1} for emeraldine base to 10^{0}−10^{1} S cm^{-1} for emeraldine salt after acid protonation.[53−57] Thus, differences in the conductivity of the polymers are not the performance-limiting factor in this case. With PPAN, PAN, and PANI already satisfying two properties mentioned in Figure 1, we therefore investigate the three polymers with respect to the three remaining criteria, namely, interfacial adhesion, mechanical elasticity, and ionic conductivity. We have found that, although PAN exhibits high interfacial adhesion with Si and PANI demonstrates good mechanical elasticity, only PPAN displays superior properties with respect to all three metrics. We then evaluate the electrochemical performance of these three composite anodes with Si through galvanostatic charge−discharge cycling experiments. The results confirm that PPAN outperforms PAN and PANI by achieving a higher capacity retention during electrochemical cycling experiments, thereby demonstrating that the interfacial, mechanical, and ionic conduction properties of the binder play key roles in determining the battery performance. The ordered stacking of individual PPAN chains near the Si surface is essential to achieving high performance, suggesting that performance could be further improved if the stacked orientation can be maximized during anode synthesis.

2. METHODS

2.1. Computational Methods. We use a ReaxFF force field developed in our previous work[48] to study interactions in Si/C/N/H systems to evaluate the interfacial and mechanical properties of the three battery binders. Here, we extend this parameter set to also describe the interactions of Li with C/N/H polymers, which allows us to evaluate the ionic conduction through the binders. All MD simulations in this work are performed using the Large-scale Atomic/Molecular Massively Parallel Simulator (LAMMPS, 12 Dec 2018 version).[58] A Nose−Hoover[59] thermostat and barostat with damping parameters of 100 and 1000 fs, respectively, are applied to control the temperature and pressure in all simulations. A timestep of 0.25 fs is used for the time integration of the equations of motion. The

https://doi.org/10.1021/acsami.1c08484
ACS Appl. Mater. Interfaces 2021, 13, 41956−41967

chemical structures of the binders used in the simulations are shown in Figure 2. Each polymer chain has 20 monomers (or 20 N atoms),

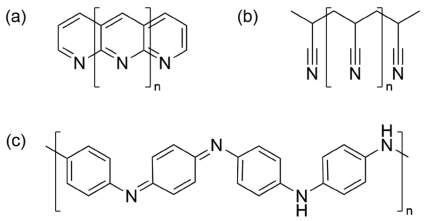

Figure 2. Chemical structures of polymer binders: (a) PPAN, (b) PAN, and (c) PANI.

which we determined in our previous work[48] to be appropriate for describing key binder properties. For PPAN, we use a cyclized aromatic structure that has been adopted in several studies as an adequate representation of the polymer's pyrolyzed structure.[42,27,60,61] PANI is represented by its common emeraldine form.[62] Test simulations with the pernigraniline form of PANI (PANIp), included in Figure S2 of the Supporting Information, yield similar results to those conducted with the emeraldine form. For all MD simulation results presented in this work, we perform five runs with different initial arrangement of the polymers to sample various configurations.

2.1.1. Simulations for Interfacial Adhesion Properties. The interfacial adhesion energy between the Si surface and the binder is evaluated using eq 1:

$$E_{\text{adhesion}} = E_{\text{Si/binder}} - E_{\text{binder}} - E_{\text{Si}} \quad (1)$$

where $E_{\text{Si/binder}}$, E_{binder}, and E_{Si} are the energies of the Si/binder composite, the binder, and the Si surface, respectively. These energies are calculated from single-point snapshots of the Si/binder configuration sampled from the MD simulations described below. For PPAN and PAN we use adhesion data reported in our previous study,[48] and here we follow the same procedure to obtain the corresponding data for PANI.

We determine the adhesion energies for the adhesion of both single chains and the bulk polymer to the Si surface. For the single-chain adhesion, a chain of the polymer is placed at a random position and orientation with respect to a (20 × 20) Si (100) surface slab, containing 24 layers of Si atoms (i.e., 9600 Si atoms). MD is performed at 300 K in an NVT ensemble, and periodic boundary conditions are applied in all three directions. The unit cell has a dimension of 76.46 Å × 76.46 Å × 150.0 Å. A sufficient vacuum of 150.0 Å is chosen between the periodic Si slabs to ensure that the single chain of the polymer interacts only with one side of the Si slab, and additionally, reflective boundary conditions are applied in the direction perpendicular to the Si surface. The interfacial energies are determined using system snapshots taken at 25 ps intervals from a 500 ps simulation that followed a ∼500 ps equilibration period.

For bulk polymer adhesion simulations, we use an (8 × 8) mirrored Si (100) surface with 24 layers (i.e., 1536 Si atoms). The Si surface has dimensions of 30.57 Å × 30.57 Å. First, the bulk polymer slab is constructed with the same surface dimensions as Si and then it is placed next to the Si surface slab. The calculated bulk polymer densities from the Si/C/N/H force field[48] are reported in Table S2 of the Supporting Information, and they are within ∼10% of the values reported in the literature. Periodic conditions are applied to the Si/binder composite unit cell in all three directions. An initial separation of 2.2 Å between the binder and Si surfaces is applied to avoid bonding artifacts that can occur if atoms are initially placed too close to one another. The composite Si/binder system is first equilibrated at 300 K in an NVT ensemble. Then, a high pressure of 5000 atm is applied in all three directions under an NPT ensemble to gradually eliminate the initial 2.2 Å separation between the binder and the Si surface. Equilibration is determined by tracking the convergence of interfacial adhesion energies calculated every 25 ps using eq 1. More details regarding the simulation procedure are available in our previous work.[48]

2.1.2. Simulations for Mechanical Properties. We follow a similar procedure as described in our previous work to calculate the Young's modulus of the three binders.[48] First, a periodic bulk binder system is constructed from 25 polymer chains placed in a large simulation box such that the initial density of the polymer is 0.01 g cm^{-3}. After an initial energy minimization is performed using the conjugate gradient method, a high temperature (500 K) and high pressure (5000 atm) annealing procedure is followed to obtain the bulk phase of the polymer. The bulk polymer structure is finally equilibrated at a temperature of 300 K and a pressure of 1 atm. The Young's modulus is calculated by applying a uniaxial tensile strain on the equilibrated bulk binder in x, y, and z directions at a constant strain rate of 10^9 s^{-1}. The polymer is stretched in one dimension at a time and the other two dimensions are allowed to deform in the NPT ensemble at 1 atm pressure. For each strained dimension, the respective stress is measured for five different samples. The average stress is then plotted as a function of the strain in the binder. The slope of the stress−strain curve in the linear elastic regime yields the Young's modulus of a binder.

To gauge the deformability of binders, we perform another set of simulations by linearly increasing the uniaxial compressive stress from 1 atm to 5000 atm over 50 ps and then equilibrating the system at 5000 atm for 250 ps. The other two dimensions are constrained to model the limiting case of a highly stressed polymer system. These simulations are performed for five different geometries for each binder and for each binder geometry, and the uniaxial stresses are applied in each of the three x, y, and z directions.

2.1.3. Simulations for Ionic Conduction Properties. To evaluate Li-ion conduction through the polymers, we extend our Si/C/N/H force field to include interactions between Li ions and C/N/H-based binders. To train the new Si/C/N/H/Li force field, we use the previous Li/C/H force field[39] training data in conjunction with our newly developed training data that include the binding energies and migration barriers of Li within C/N/H-based polymers as well as bond dissociation energies of Li−N bonds in several C/N/H/Li molecules. Full details of the training procedure are provided in the Supporting Information.

For each binder, the Si/binder composite are constructed following a procedure similar to the one used for the bulk interfacial adhesion simulations described above. Nonperiodic reflective boundary conditions are applied in the direction perpendicular to the Si/binder interface (z direction), and a vacuum region of 150 Å is added while equilibrating the composite structures. After equilibration, 1240 Li atoms are randomly placed in the vacuum region within 30 Å from the top of the binder atoms, corresponding to the bulk density of Li. This construction leads to a nonperiodic Si/binder/Li composite structure where a vacuum region of ∼120 Å is present to avoid interaction between Li and the underside of the Si slab, thus allowing Li atoms to migrate through the binder toward the Si surface. A sample structure for each binder composite is shown in Figure S5 in the Supporting Information. An initial energy minimization using the conjugate gradient method is performed to allow local relaxation of the constructed composite structure. This is followed by an MD simulation in NVT ensemble at 300 K for 200 ps, where the positions of Li atoms are tracked and analyzed.

2.2. Experimental Methods. *2.2.1. Work of Adhesion of Si/Polymer Interfaces from Contact Angle Measurements.* The work of adhesion between Si and the polymer surfaces (PPAN, PAN, and PANI) is determined using contact angle measurements.[63] Thin films of polymers on glass slides are prepared as follows: PAN (M_w ≈ 150,000, Sigma-Aldrich) is dissolved in *N*,*N*-dimethylformamide (DMF, ≥99.9%, Sigma-Aldrich) and spin-coated onto glass slides. The PPAN samples are obtained by further heating the PAN-coated glass slides under an inert argon atmosphere at 280 °C for 30 min and 550 °C for 30 min. On the other hand, PANI is synthesized from aniline monomers (≥99.5%, Sigma-Aldrich) using ammonium persulfate (≥98%, Sigma-Aldrich) as the oxidizer and phytic acid (50% w/w in H_2O, Sigma-Aldrich) as both the dopant and cross-

https://doi.org/10.1021/acsami.1c08484
ACS Appl. Mater. Interfaces 2021, 13, 41956−41967

linker.[21,32,52] The reacting mixture is drop-casted onto glass slides and allowed to fully polymerize overnight. The PANI-coated glass slides are then thoroughly rinsed with DI water to remove excess reactants (Figure S6). Contact angles of different probe liquids on the various polymer-coated surfaces (PAN, PPAN, and PANI) as well as on a reference Si surface are individually measured (Table S4). A Si wafer (Silicon Sense, Inc.) is used for the reference Si surface. Surface free energy values and components of these probe liquids are provided in Table S5. Surface free energy components of the solid surfaces are then calculated from these measurements by either applying the Owens, Wendt, Rabel, and Kaelble (OWRK) method (using a combination of two probe liquids, eq 4) or the Oss and Good acid–base method (using a combination of three probe liquids, eq 6). Work of adhesion between the Si and polymer surfaces (Si/PPAN, Si/PAN, and Si/PANI) is then derived from the calculated solid surface free energies using either eq 5 or eq 7. Since the surface free energy components of the solids and the resulting work of adhesion are highly dependent on the choice of probe liquid combinations, the different values of work of adhesion are summarized in Table S6.

$$\gamma = \gamma^{d} + \gamma^{p} \tag{2}$$

$$\gamma^{p} = 2\sqrt{\gamma^{+}\gamma^{-}} \tag{3}$$

$$\gamma_l(1 + \cos\theta) = 2\left(\sqrt{\gamma_l^{d}\gamma_s^{d}} + \sqrt{\gamma_l^{p}\gamma_s^{p}}\right) \tag{4}$$

$$W_a = 2\left(\sqrt{\gamma_1^{d}\gamma_2^{d}} + \sqrt{\gamma_1^{p}\gamma_2^{p}}\right) \tag{5}$$

$$\gamma_l(1 + \cos\theta) = 2\left(\sqrt{\gamma_l^{d}\gamma_s^{d}} + \sqrt{\gamma_l^{+}\gamma_s^{-}} + \sqrt{\gamma_l^{-}\gamma_s^{+}}\right) \tag{6}$$

$$W_a = 2\left(\sqrt{\gamma_1^{d}\gamma_2^{d}} + \sqrt{\gamma_1^{+}\gamma_2^{-}} + \sqrt{\gamma_1^{-}\gamma_2^{+}}\right) \tag{7}$$

where γ_l and γ_s are the surface free energies of liquid and solid, respectively; γ^{d}, γ^{p}, γ^{+}, and γ^{-} are the dispersive, polar, acid, and base components of surface free energy, respectively; θ is the contact angle between probe liquid and solid; γ_1 and γ_2 are the surface components corresponding to materials 1 and 2; and W_a is the work of adhesion between materials 1 and 2.

2.2.2. Electrochemical Characterization. 2.2.2.1. Electrode Fabrication. The Si/PAN anode is fabricated by mixing Si nanoparticles (<100 nm particle size, Sigma-Aldrich), PAN, and conductive carbon additive (Super C65, TIMCAL) at a mass ratio of 70:20:10 using DMF as the solvent. The well-sonicated and well-mixed slurry is spray-coated onto copper foil (MTI Corp.) with an airbrush (Model G22, Master Airbrush) and dried under vacuum. The Si/PPAN anode is prepared in a similar fashion, except with a Si:PAN ratio of 70:30 and without the addition of conductive carbon. The electrode sheet is subsequently heated under an inert argon atmosphere at 280 °C for 30 min and 550 °C for 30 min. As reported earlier, this pyrolysis step converts the PAN into its conjugated form, increasing the electrical conductivity of the final Si/PPAN electrode.[16,27−29] The fabrication of the Si/PANI anode[21] involves mixing the Si nanoparticles with a solution containing aniline monomers and phytic acid (serving as both the dopant and cross-linker). Ammonium persulfate solution is then added into the mixture to initiate polymerization. After ∼1 min sonication, the viscous dark green mixture is cast onto copper foil through doctor blading (Automatic Film Coater, AFA-III, MTI Corp.). The final Si/PANI electrode is then thoroughly rinsed with DI water to remove excess reactants, calendered (Roller Press, HRP-MR100B, MTI Corp.), and dried under vacuum. The wt % of Si in Si/PANI is calculated to be 70%. All three Si/PAN, Si/PPAN, and Si/PANI electrode sheets are punched into disks 12.7 mm in diameter for use in coin-cell testing. The total mass loading for each tested sample is ∼1.0 mg cm^{-2}.

2.2.2.2. Coin Cell Assembly and Electrochemical Testing. Half-cell tests are performed using coin cells (CR2032, MTI Corp.) with Celgard 2325 PP/PE separators and Li foil counterelectrodes. The electrolyte consists of 1 M $LiPF_6$ (Strem Chemicals, Inc.) dissolved in ethylene carbonate/diethylene carbonate (EC/DEC):dimethyl carbonate (DMC):fluoroethylene carbonate (FEC) at a 2:1:1 w/w ratio (Novolyte Technologies Inc.). All cells are assembled in an argon glove box (Innovative Technologies Inc.) with O_2 and H_2O levels below 0.2 ppm. All battery tests are performed on an Arbin Instruments BT-2143 tester at room temperature. For the calculation of Li-ion diffusion coefficients, coin cells undergo one formation cycle at 0.1 A g^{-1} and subsequent cyclic voltammetry experiments between 0.01 and 1.2 V at various scan rates from 0.025 to 0.4 mV s^{-1}. The Randles–Sevcik equation is applied:[64,65]

$$i_p = 2.69 \times 10^5 n^{3/2} A D^{1/2} C v^{1/2} \tag{8}$$

where i_p is the peak current in A, $n = 1$ is the number of electrons transferred per one Li^+, A is the electrode area in cm^2, D is the diffusion coefficient in cm^2 s^{-1}, C is the concentration of Li^+ in mol cm^{-3}, and v is the scan rate in V s^{-1}. The diffusion coefficient is obtained from the slope of the linear relationship between the peak current and the square root of the voltage scan rate. For the galvanostatic charge–discharge study, coin cells are cycled at 0.1 A g^{-1} between 0.01 and 1.0 V for five formation cycles before the current rate is increased to 0.5 A g^{-1} for later cycles.

2.2.3. Morphology Characterization. The morphologies of the Si/PPAN, Si/PAN, and Si/PANI electrodes before and after electrochemical cycling are analyzed with scanning electron microscopy (SEM) using an FEI Helios NanoLab 660 DualBeam system. The electron beam is configured with a low voltage of 1 kV and a beam current of 25 pA to minimize sample damage. To further reduce the charging effect, all samples are coated with a thin layer of Au using a Denton Desk V sputter system before SEM imaging.

3. RESULTS

3.1. Interfacial Adhesion Properties of Polymer Binders. Interfacial adhesion properties of single chains of polymer binders are evaluated first to determine their affinity for the Si surface. The interfacial adhesion energy between a single polymer chain and the Si surface is calculated using eq 1. For each of the three polymers, five independent initial geometries are created with the random placement of the single polymer chain over the Si surface. The average interfacial adhesion energy of polymer chains from the five independent simulations is shown in Figure 3a for the three polymer binders. These results show that among the three binders, PANI chains have the highest affinity to the Si surface. This is also evident from the geometry of the PANI chain when it is adhered to the Si surface (Figure 3c). The mixed parallel/perpendicular orientation of the PANI chain allows more bonds to form at the interface compared to PPAN and PAN, where the perpendicular orientation of the chain allows fewer bonds to form.

Work of adhesion from contact angle experiments is calculated for each binder to validate the observations from the single chain/Si MD simulations. In these experiments, the interaction between Si and a binder is determined through measured contact angles with probe liquids. A higher work of adhesion indicates that more force is required to separate Si and the binder. Although these experiments do not measure the direct interfacial adhesion between Si and the binder, they can still predict the affinity of binders for the Si surface and have been used widely for similar analyses.[63] We perform these experiments with eight different combinations of probe liquids for each of the binders (Table S6) and report the average work of adhesion in Figure 3b. We plot the negative of the work of adhesion in Figure 3b to qualitatively compare these results with the interfacial adhesion energies computed from simulation. The agreement between simulation and experiment reaffirms the stronger affinity of PANI chains to the Si surface

https://doi.org/10.1021/acsami.1c08484
ACS Appl. Mater. Interfaces 2021, 13, 41956−41967

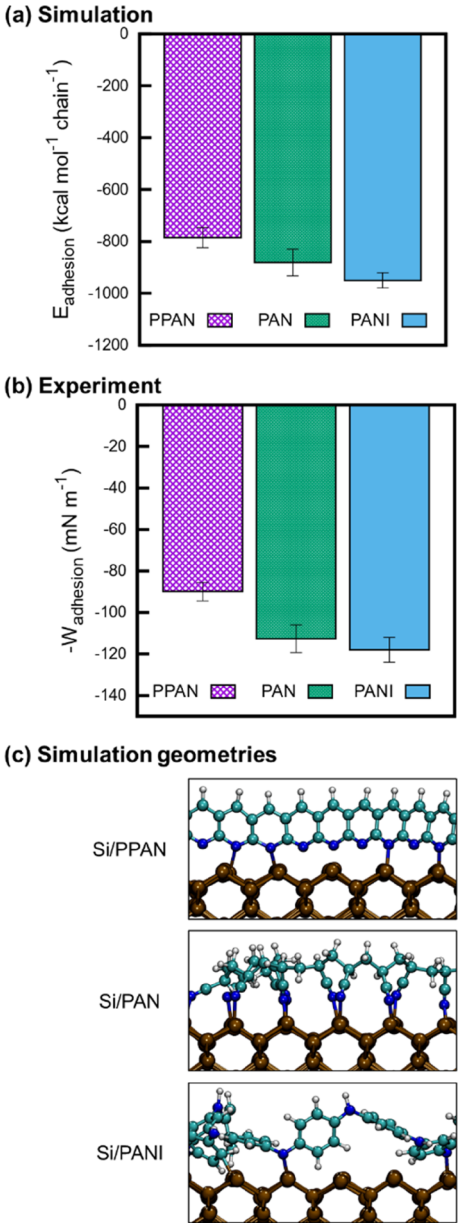

Figure 3. (a) Interfacial adhesion energies of a single chain of polymers on the silicon surface obtained from MD simulations. The error bars represent standard error from five simulations. The data for PPAN and PAN is from our previous work.[48] (b) Negative of the work of adhesion of polymers on the silicon surface obtained from experiments. The error bars represent standard error from eight experiments. (c) Geometries of single chains of polymers adhered to the silicon surface obtained from MD simulations. Brown: Si, turquoise: C, blue: N, white: H.

and also validates our simulation methods and the Si/C/N/H force field.[48]

Having determined the affinity of polymer chains to the Si surface, we next determine the direct interfacial interaction of the bulk polymer with the Si surface, taking inspiration from our previous work.[48] Using the simulation workflow described in the Methods section, we determine the bulk interfacial adhesion energies for all three polymers by eq 1. Biases resulting from the initial orientation of bulk polymers with the Si surface are minimized by sampling five independent polymer geometries with random placement of the polymer chains. The average interfacial adhesion energies from the five samples for each of the three polymer binders are shown in Figure 4a along

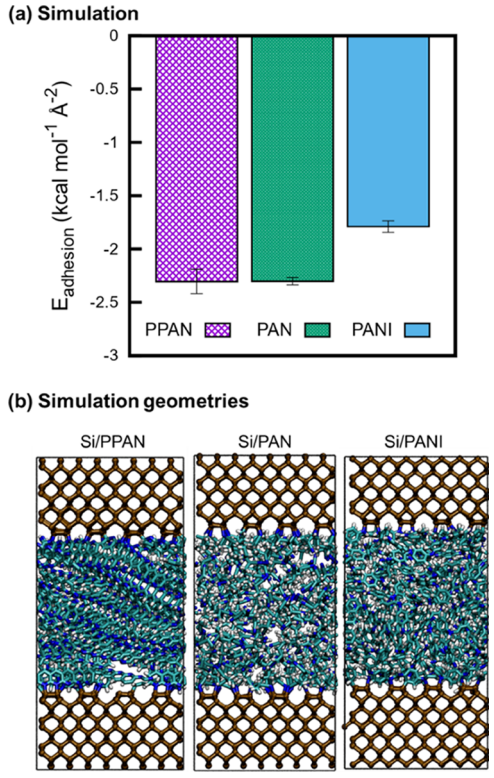

Figure 4. (a) Interfacial adhesion energies of bulk polymer binders with the silicon surface obtained from MD simulations. The error bars represent standard error from five simulations. The data for PPAN and PAN is from our previous work.[48] (b) Geometries of bulk polymers adhered to the silicon surface obtained from MD simulations. Brown: Si, turquoise: C, blue: N, white: H. Reprinted with permission from ref 48. Copyright 2019 American Chemical Society

with the final geometries of one of the samples for each Si/binder composite (Figure 4b). A trend emerges that is opposite to what is expected from the results of the single-chain adhesion simulations and work of adhesion experiments (Figure 3a,b). The trend reversal shows that PANI bulk does not adhere strongly to the Si surface compared to PPAN and PAN. Thus, the behavior of a single chain is not necessarily indicative of the bulk polymer.

The cause for the adhesion energy trend reversal is examined by analyzing the structural features of Si/polymer interfaces obtained from MD simulations of bulk Si/PPAN and Si/PANI composites. We perform a similar analysis to our previous work[48] to explain this trend reversal in Si/PPAN and Si/PPy composites. Details of the analysis are provided in the Supporting Information. We investigate the orientation of bulk polymer chains with the Si surface (Figure 5a,b) and the distribution of these chains in the direction normal to the Si surface (Figure 5c,d) over the course of simulation. Since PAN does not have aromatic rings like PPAN and PANI, the orientation of PAN chains cannot be defined, and therefore, we do not consider PAN in this analysis. As shown in Figure 5a, the PPAN chains at the interface reorient themselves during the simulation to align perpendicular to the surface, similar to the orientation of a single PPAN chain over Si (Figure 3c).

https://doi.org/10.1021/acsami.1c08484
ACS Appl. Mater. Interfaces 2021, 13, 41956−41967

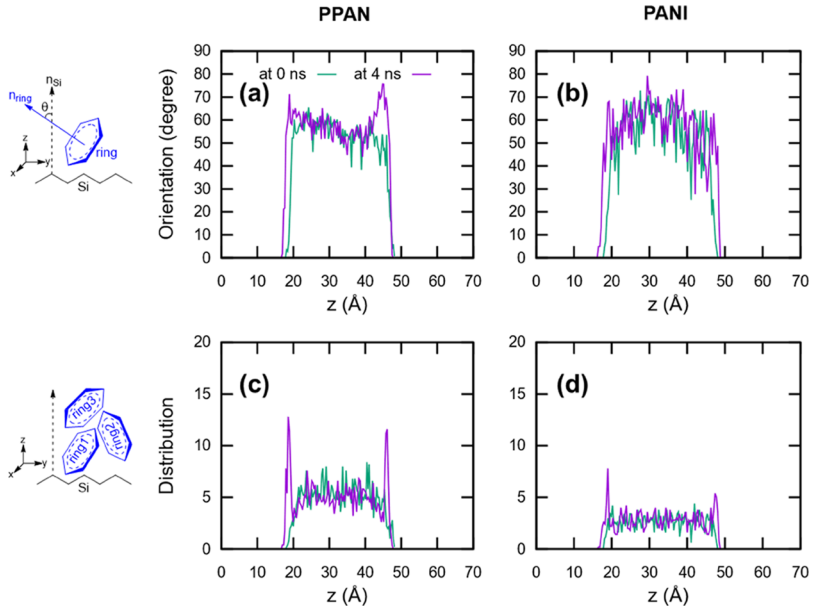

Figure 5. (a, b) Orientation of monomers of (a) PPAN and (b) PANI with respect to the Si surface at the start (green) and end (violet) of the MD simulation. (c, d) Distribution of the monomers of polymers (c) PPAN and (d) PANI in the direction perpendicular to the Si surface at the start (green) and end (violet) of the MD simulation. The data for PPAN is from our previous work.[48] (Panels (a,c) are reprinted with permission from ref 48. Copyright 2019 American Chemical Society)

This perpendicular orientation leads to ordered stacking of PPAN chains, which results in a higher number of chains being able to bind to the Si surface, as evident in Figure 5c. On the other hand, PANI chains at the interface have a random and mixed orientation with poor ordering (Figure 5b), similar to the orientation of a single PANI chain over Si (Figure 3c). The mixed orientation features more bound chains that are parallel to the surface and occupy more interfacial area, which allows fewer chains to bind to the surface, as reflected in Figure 5d. These results clearly explain the trend reversal, where the stronger affinity of individual PANI chains is not translated to the bulk Si/PANI composites because of a poorer ordering of those chains at the interface. PPAN chains, although having a weaker individual affinity to Si, bind perpendicularly to the surface, resulting in better stacking and higher overall adhesion in bulk Si/PPAN composites. These simulation results suggest that the weakly bound Si particles in Si/PANI composites would agglomerate more than in the other two composites, thus degrading the anode faster.

To confirm this prediction about particle agglomeration, we analyze the SEM images of the composite Si/binder anode materials in Figure 6. While all three Si/PPAN, Si/PAN, and Si/PANI anodes have small particles in their pristine condition, suggesting good initial dispersion and confinement of Si nanoparticles within their respective polymer matrices right after synthesis, only the Si/PPAN and Si/PAN anodes are able to retain the small particle size after electrochemical cycling, compared to the large particles visible in the Si/PANI anode after cycling. The change in particle size after cycling is an indicator of the strength of the interaction between the bulk polymer and the Si surface. A stronger interfacial interaction maintains Si/binder interfaces throughout the cycling and limits the mobility and agglomeration of Si particles. Weaker Si/binder interaction facilitates the agglomeration of Si particles during cycling and results in a loss of active Si material, ultimately hampering the battery performance. Clearly, the retention of smaller particle sizes and uniformly

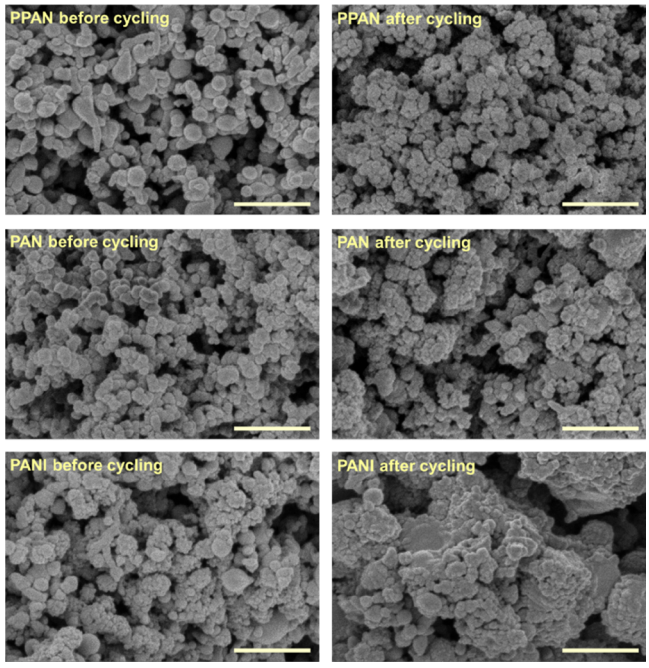

Figure 6. SEM images of Si/binder composite anodes before and after electrochemical cycling (all scale bars represent 500 nm).

dispersed particles in Si/PPAN and Si/PAN anodes throughout cycling is the result of stronger adhesion energies caused by ordered interfacial stacking, while the opposite happens to Si/PANI where cycling leads to agglomeration because of weaker adhesion between Si and the binder. This validates the prediction from our simulations and shows that the configurational characterization of interfacial structures is essential for selecting binders with strong interfacial adhesion properties.

3.2. Mechanical Properties of Polymer Binders. The mechanical properties of the binder play an important role in reducing lithiation-induced stress in Si to maximize lithium

https://doi.org/10.1021/acsami.1c08484
ACS Appl. Mater. Interfaces 2021, 13, 41956−41967

uptake and active material utilization. We evaluate the mechanical properties of the binders by first calculating their Young's modulus, which is a measure of the stiffness of the binder. The standard MD procedure, as applied in our previous work,[48] is utilized here to measure stress as a function of applied tensile strain. The Young's moduli of the three binders obtained from the stress−strain curves are reported in Table 1. Similar experimental evaluation was not necessary, as

Table 1. Comparison of Young's Modulus of the Three Binders Calculated from Simulations Using the Si/C/N/H Force Field[48] and Respective Values from the Literature[a]

	Young's modulus (GPa)	
binder	Si/C/N/H force field[48]	literature
PPAN	1.2	1.3[66]
PAN	6.0	6.3[67]
PANI	2.6	1.3[68]

[a]The data for PPAN and PAN is from our previous work.[48]

experimental data for these three binders are already available.[66−68] The values calculated from MD compare well with the values reported in the literature. These results show that PPAN is the most elastic and PAN is the stiffest binder. The PPAN chain has aromatic rings attached through conjugated π bonds (Figure 2), restricting the rotation and bending of the chain. In PANI, the aromatic rings are attached through σ bonds, allowing more rotation and bending of the chain. In PAN, most atoms are bonded through σ bonds, allowing the highest degree of rotation and bending in the chain. More rotation and bending within the individual polymer chains result in coiling and entanglements of chains, which lead to less elastic bulk polymer structures. A comparison of the structures of bulk PPAN, PANI, and PAN in Figure 7 demonstrates this phenomenon, where the bending and coiling of individual chains increase from bulk PPAN to bulk PAN. These structural differences explain the differences in the stiffness of binders, where more ordered and less coiled PPAN chains would slide over one another to relieve stress upon deformation.

Another mechanical property of interest is the ability of the binders to deform under the application of compressive stress. To assess this, we apply uniaxial compressive stress to the bulk polymer and measure the resulting strain. This procedure mimics the lithiation-induced deformation in Si/binder composites, where Si applies compressive stress to the binder upon lithiation and the deformability of the binder controls the ease of lithiation. In principle, a deformable binder would allow for a higher degree of lithiation in Si. Uniaxial deformation MD simulations are performed following the procedure described in the Methods section on five samples for each of the binders. The average strains in the binders measured from these simulations are shown in Figure 8. PAN undergoes a smaller amount of deformation as compared to the other two binders. This trend is similar to the one that we obtain from the Young's modulus calculations. These results demonstrate that, among the three binders, PPAN is the most deformable binder, and thus is a suitable candidate for Si anodes based on mechanical properties.

3.3. Ionic Conductivity of Polymer Binders. Facile conduction of Li ions through polymer binders is desirable to minimize the resistive losses and maximize energy efficiencies in battery electrodes. MD simulations are performed to

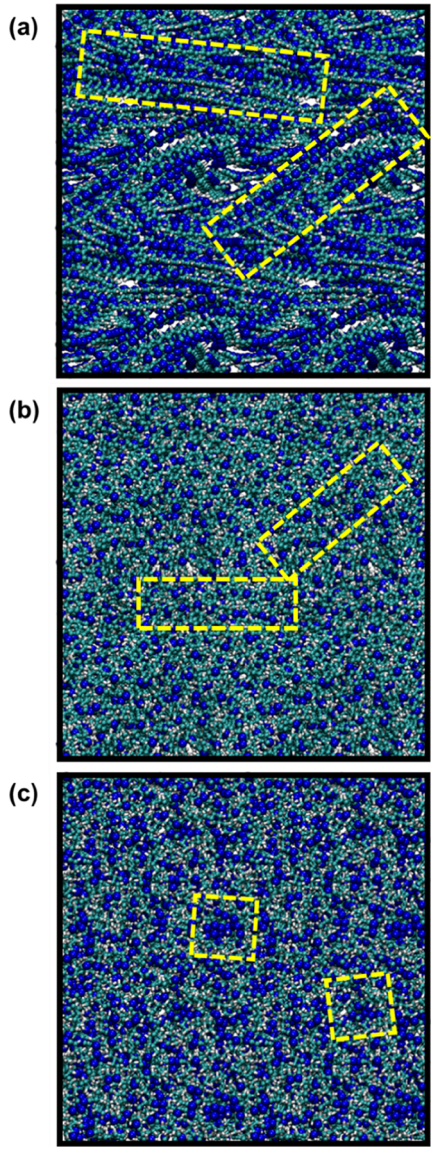

Figure 7. Structures of bulk binders: (a) PPAN, (b) PANI, and (c) PAN. The yellow boxes show examples of individual chains with increasing bending and coiling from PPAN to PAN. For better visualization of chains, the radius of nitrogen atoms has been increased. Turquoise: C, blue: N, white: H.

evaluate the Li-ion migration through binders. The positions of all the Li atoms are tracked during the simulation, and the z-coordinate of the lowest single Li atom and the z-coordinate of the center of mass (COM) of all the Li atoms at each timestep are determined (Figure 9). The z-coordinate of the lowest Li atom and that of the COM continuously decrease for all the Si/binder systems, indicative of Li migration to the Si/binder interface driven by the Li concentration gradient. The rate of Li-ion migration is different depending on the polymer, where PPAN conducts Li more rapidly than the other two polymers. As shown in Figure 9a, the Li atoms reach the Si interface more quickly for PPAN compared to PAN and PANI. This is also evident from the snapshots of the three systems at the end of the MD simulation (Figure 10). Since the position of the single lowest Li atom does not represent the mobility of the entire group of atoms, we also look at the collective dynamics of all the Li atoms by calculating the z-coordinate of the COM

https://doi.org/10.1021/acsami.1c08484
ACS Appl. Mater. Interfaces 2021, 13, 41956−41967

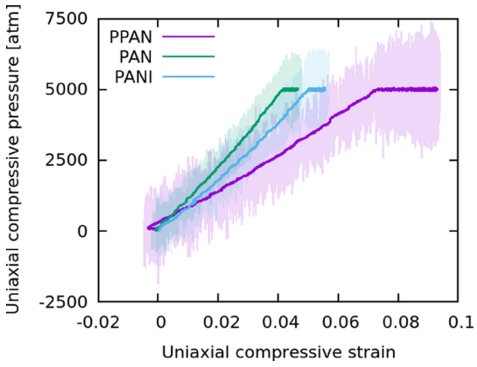

Figure 8. Uniaxial compressive strain in bulk polymer binders as a function of uniaxial compressive pressure. The shaded regions represent the actual data, and the solid lines are the moving average of the actual data. For each binder, the results represent an average over five geometries and for each geometry an average over three directions.

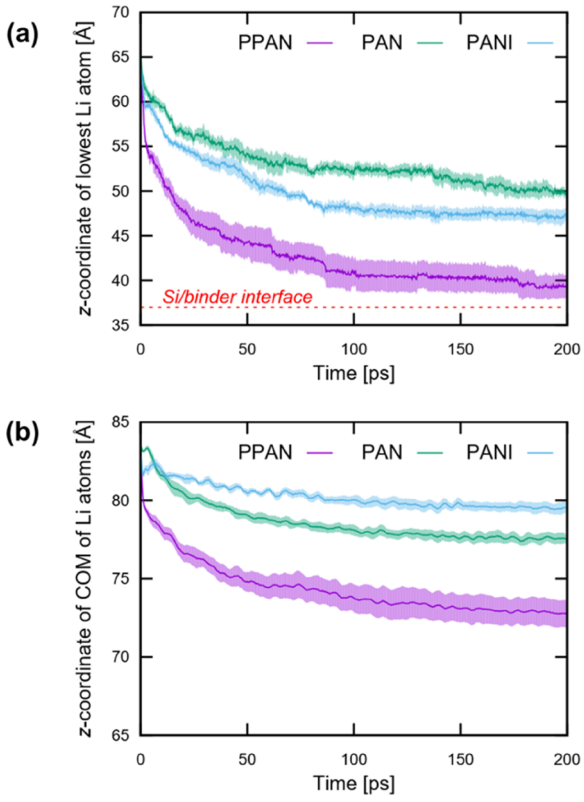

Figure 9. *z*-coordinate of (a) lowest Li atom and (b) center of mass (COM) of all Li atoms during the MD simulation of the Si/binder/Li composite. The red dashed line represents the Si/binder interface at 37 Å. The dark solid lines and the shaded regions in these plots represent the average and standard error from five simulations for each binder, respectively.

of Li atoms in Figure 9b. Here, we find that the overall Li-ion conduction is much faster in PPAN followed by PAN and then PANI. There are structural channels present in PPAN (represented by the white arrow in Figure 10) that form because of its ordered stacking near the Si/polymer interface (Figure 5), which promotes faster Li-ion transport. These channels do not form as readily in PAN and PANI, and thus these polymers exhibit slower Li-ion transport.

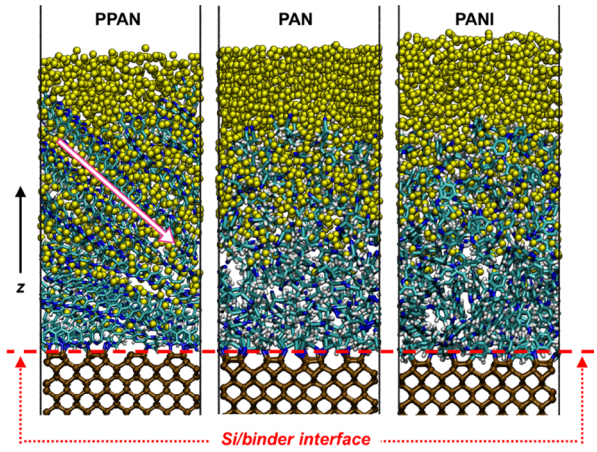

Figure 10. Snapshots of Si/binder/Li systems for PPAN, PAN, and PANI polymers at the end of MD simulations after 200 ps. The white arrow in the PPAN structure highlights one of the Li-ion conduction channels that form in PPAN. Brown: Si, turquoise: C, blue: N, white: H, yellow: Li.

To test our predictions from simulation, Li-ion diffusion coefficients for Si/PPAN, Si/PAN, and Si/PAN are experimentally obtained from cyclic voltammetry measurements of the respective half-cells with Li foil at various scan rates (Figure S7). The first cathodic peak current versus the square root of the voltage sweeping rate shows a linear relationship for each composite (Figure S8). Through the application of the Randles–Sevcik equation (eq 8), Li-ion diffusion coefficients are calculated for the three Si/polymer composite electrodes, summarized in Table 2. The Si/PPAN composite demonstrates a significantly higher Li-ion diffusion coefficient compared to those of Si/PAN and Si/PANI, while Si/PANI has the lowest coefficient among the three samples. These experimental results align well with the previous MD simulation results shown in Figure 9b, in which Li-ion conduction is the fastest in PPAN followed by PAN and then PANI. A key feature explaining Si/PPAN's superior Li-ion conductivity is the ordered stacking of the polymer chains at the interface with Si, which provides structural channels favorable for fast Li-ion migration.

Table 2. Li-Ion Diffusion Coefficients for Si/PPAN, Si/PAN, and Si/PANI Obtained from Cyclic Voltammetry Tests

sample	Li-ion diffusion coefficients in $cm^2\ s^{-1}$
Si/PPAN	444.9×10^{-9}
Si/PAN	36.5×10^{-9}
Si/PANI	7.1×10^{-9}

3.4. Galvanostatic Charge–Discharge Study of Si/Polymer Composite Anodes. For comparing the cycling performance of Si/PPAN, Si/PAN, and Si/PANI electrodes, half-cells with Li foil are cycled at 0.1 A g^{-1} between 0.01 and 1.0 V for five formation cycles before the current rate was increased to 0.5 A g^{-1} (Figure 11). For the first cycle, Si/PPAN demonstrates the highest discharge and charge capacities of 2223.8 and 1751.9 mAh g^{-1}, respectively, resulting in the highest Coulombic efficiency of 78.8%. In comparison, Si/PAN shows the first-cycle discharge and charge capacities of 1104.0 and 656.9 mAh g^{-1}, respectively, resulting in a significantly lower Coulombic efficiency of 59.5%. Finally,

https://doi.org/10.1021/acsami.1c08484
ACS Appl. Mater. Interfaces 2021, 13, 41956–41967

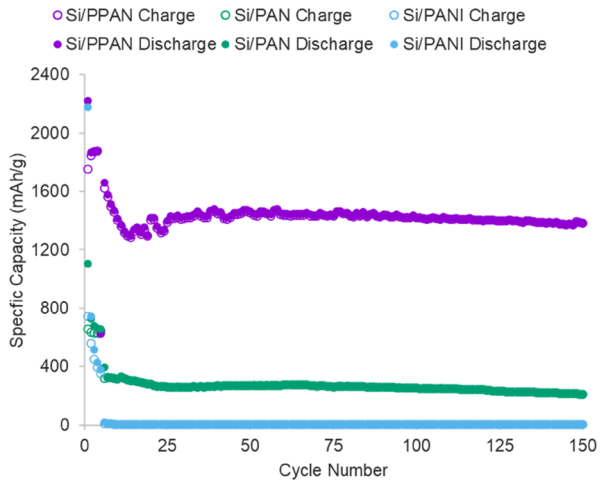

Figure 11. Cycling performance of Si/PPAN, Si/PAN, and Si/PANI half-cells.

Si/PANI obtains a high first-cycle discharge capacity of 2177.6 mAh g^{-1}, closely matching that of Si/PPAN, but has a considerably lower first-cycle charge capacity of only 745.3 mAh g^{-1}, resulting in the lowest Coulombic efficiency of 34.2%. While both Si/PPAN and Si/PAN can roughly maintain their charge capacities for the first five formation cycles, Si/PANI has its charge capacity reduced rapidly to 352.7 mAh g^{-1} at cycle 5. As the current rate is increased to 0.5 A g^{-1} for cycle 6 and later, the capacities of all three composites fade, with Si/PPAN and Si/PAN stabilizing at ~1450 and ~250 mAh g^{-1}, respectively. Notably, the capacity of Si/PANI at this higher current rate becomes negligible, averaging only ~5 mAh g^{-1}. Overall, Si/PPAN demonstrates substantially superior capacity retention, which can be attributed to its favorable properties across all three criteria under investigation: strong interfacial adhesion, high mechanical elasticity, and fast ionic conduction.

4. DISCUSSION

PPAN outperforms PAN and PANI as a binder for Si-based electrodes because it combines strong interfacial adhesion with a high mechanical elasticity and high ionic conduction, as summarized in Table 3. We also discover that better properties and performance of the Si/PPAN composite are a result of its morphology at the interface and in the bulk polymer phase, thus equipping us with a tool to optimize other binders and guide the experimental design of such composites. The structural ordering of PPAN chains in the bulk polymer phase allows individual chains to slide over one another during deformation, thus improving the mechanical elasticity. The perpendicular orientation of PPAN chains at the Si/binder interface also strengthens the bonding of Si to PPAN due to ordered and dense coverage of the polymer over the Si surface. In addition, the ordering of PPAN chains enables ion-conducting pathways that promote faster Li conduction through PPAN.

Table 3. Summary of the Results Showing that PPAN is a Suitable Binder for Si-Based Anodes in Li-Ion Batteries owing to its Superior Interfacial Adhesion, Mechanical Elasticity, and Ionic Conductivity

	PPAN	PAN	PANI
Interfacial Adhesion	✓ Strong	✓ Strong	✗ Weak
Mechanical Elasticity	✓ High	✗ Low	✓ High
Ionic Conductivity	✓ High	✗ Low	✗ Low

Despite excelling in all property metrics, we believe that PPAN can still be further optimized. The standard error in Li conduction from the five independent simulations, represented by the shaded region in Figure 9, is higher in the case of PPAN compared to the other two polymers because some of the independent bulk PPAN structures allow faster Li-ion conduction compared to others. The differences in the orientation of these channels in different PPAN samples, as shown in Figure S9, result in differences in the Li-ion conduction rates, leading to a higher standard error for PPAN in Figure 9. The geometries of the fastest and slowest Li-conducting samples of Si/PPAN, shown in Figure 12, demonstrate that the channels that are oriented vertically to the Si/binder interface offer shorter Li-ion migration pathways and faster conduction (the geometries of the other Si/PPAN samples are included in Figure S9 of the Supporting Information). This implies that potential improvements in performance can emerge from proper control of channel orientation. Furthermore, we determine that the highly conducting sample of Si/PPAN also has higher interfacial adhesion (Figure 12c) due to a higher concentration of PPAN chains near the Si/PPAN interface (Figure S10). The interfacial adhesion is governed by the polymer chains closer to the Si surface, while the ionic conduction is governed by the polymer chains farther away from the Si surface. Therefore, both properties can be tuned independently to optimize both ion conduction and adhesion.

In summary, the prolonged cycling of Si/PPAN electrodes serves as a proof of PPAN superior properties attributed to its structural features, thus establishing it as a promising binder that meets all important criteria for its application in next-generation Si anode-based Li-ion batteries. Such strategies of enhancing the interfacial and bulk ordering of polymers can be applied in the experimental synthesis of Si/polymer composites to achieve better electrochemical performance from the battery electrodes.

5. CONCLUSIONS

Through combined simulations and experiments to analyze the interfacial, mechanical, and ionic properties of binders (PPAN, PAN, and PANI), we establish important structure−property characteristics that are beneficial for engineering high-performing binders for Si anodes in Li-ion batteries. We analyze the adhesion properties from the perspective of the affinity of a single chain of a polymer and also as a bulk polymer near a Si interface. The results show contrasting behaviors, where PANI, having a higher affinity to Si as a single chain, fails to adhere strongly to Si in the bulk case because of its poor interfacial stacking over the Si surface compared to PPAN, which has a densely ordered structure at the interface. These results are supported well by experimental work of adhesion tests and SEM images, with the latter showing a stronger binding between Si/PPAN in the bulk case and less Si−Si particle agglomeration. Mechanically, we find that PPAN and PANI are more elastic binders than PAN based on the calculations of

https://doi.org/10.1021/acsami.1c08484
ACS Appl. Mater. Interfaces 2021, 13, 41956−41967

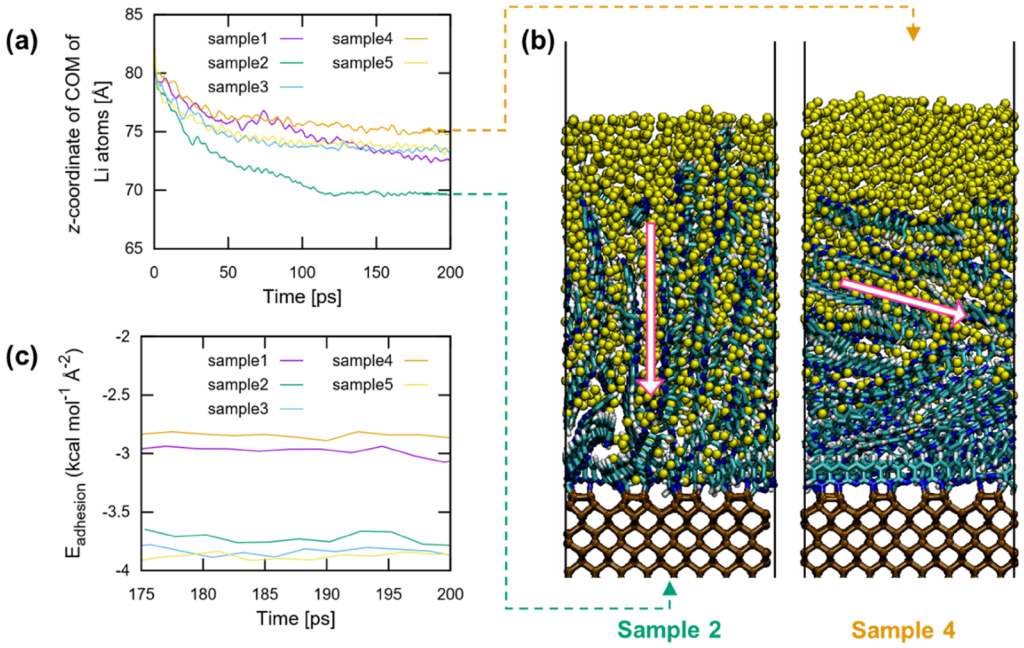

Figure 12. (a) *z*-coordinate of the center of mass (COM) of all Li atoms during the MD simulation of five samples of the Si/PPAN/Li composite. (b) Snapshots of the fastest (sample2) and slowest (sample4) Li-ion conducting PPAN samples, with white arrows depicting the direction of Li conduction channels. Brown: Si, turquoise: C, blue: N, white: H, yellow: Li. (c) Interfacial adhesion energies of these Si/PPAN samples during the last 25 ps of MD.

Young's modulus. We also test the ability of the binders to undergo deformation upon the application of compressive stress, mimicking the lithiation-induced deformation in binders. These results corroborate with the calculated Young's modulus, suggesting that PPAN can undergo substantial deformation, owing to its ordered and less coiled bulk structure. Experimentally, we also find that the Si/PPAN composite demonstrates the highest Li-ion diffusion coefficient, and simulations support these results, revealing the importance of ion-conducting channels formed in PPAN because of better structural stacking. From the evaluation of adhesion, mechanical, and ionic conduction properties, we anticipate PPAN to be a better binder than the other two. Upon performing the electrochemical cycling experiments, we find that PPAN does perform the best, retaining a capacity of ~1400 mAh g^{-1} for 150 cycles. We infer from these results that the polymers that order well in the bulk phase and at the Si/polymer interface would be better binder candidates for Si anodes.

In conclusion, this work provides a synergistic approach for binder evaluation, selection, and optimization by combining modeling with experiments. Atomistic simulations allow us to evaluate individual properties of binders in a decoupled manner and also enable us to identify important structural features that are relevant for those properties. Experiments then utilize this knowledge to test the binders, enable us to observe the direct role these properties play in battery performance, and validate the predictions from simulation. As a result, this combined approach highlights the importance of structural features such as interfacial binding modes, bulk ordering, and ion-diffusion channels that can be tuned based on atomistic insights to optimize binder properties and develop better battery electrodes. Our ongoing efforts are focused on utilizing these insights to engineer novel binders with enhanced properties by incorporating relevant functional groups and structural features. This will also involve expansion of the force field, which is currently sufficient for only C/N/H-based functional groups.

■ ASSOCIATED CONTENT

Supporting Information

The Supporting Information is available free of charge at https://pubs.acs.org/doi/10.1021/acsami.1c08484.

Cycling performance of three Si/PAN electrodes at various carbon additive contents; resistivity measurements of Si/PAN and Si/PPAN electrodes; interfacial adhesion energies of single-chain and bulk polymers of PPAN, PAN, and PANI (emeraldine and pernigraniline forms); bulk densities of polymers using MD simulations; development of Si/C/N/H/Li force field, training, and comparison with DFT; initial structures of Si/binder/Li systems for Li conduction simulations; images of in situ polymerized PANI films on glass slides; contact angles, surface energies, and work of adhesion calculated for the three polymers; analysis of the trend reversal in adhesion energy; CV tests for the three Si/binder composites and their linear fits; direction of Li-conduction channels in PPAN samples; and distribution of PPAN monomers in a strongly conducting and adhering PPAN sample and a weakly conducting and adhering PPAN sample (PDF)

■ AUTHOR INFORMATION

Corresponding Author

Thomas P. Senftle − *Department of Chemical and Biomolecular Engineering, Rice University, Houston, Texas 77005-1892, United States;* orcid.org/0000-0002-5889-5009; Email: tsenftle@rice.edu

Authors

Manav Bhati − *Department of Chemical and Biomolecular Engineering, Rice University, Houston, Texas 77005-1892, United States*

Quan Anh Nguyen − *Department of Chemical and Biomolecular Engineering, Rice University, Houston, Texas 77005-1892, United States;* orcid.org/0000-0003-1893-5085

Sibani Lisa Biswal − *Department of Chemical and Biomolecular Engineering, Rice University, Houston, Texas 77005-1892, United States;* orcid.org/0000-0002-0610-835X

Complete contact information is available at: https://pubs.acs.org/10.1021/acsami.1c08484

Author Contributions

#M.B. and Q.A.N. contributed equally to this manuscript.

Notes

The authors declare no competing financial interest.

■ ACKNOWLEDGMENTS

Q.A.N. acknowledges the support from the National Science Foundation Graduate Research Fellowship under Grant No. 1842494. M.B. acknowledges the support from the Kobayashi Fellowship at Rice University. This work was conducted in part using the resources of the Shared Equipment Authority and the Center of Research Computing at Rice University. The authors acknowledge the use of Electron Microscopy Center (EMC) at Rice University. The authors also acknowledge the financial support from the Rice Energy and Environment Initiative.

■ REFERENCES

(1) Obrovac, M. N.; Christensen, L. Structural Changes in Silicon Anodes during Lithium Insertion/Extraction. *Electrochem. Solid-State Lett.* **2004**, *7*, A93−A96.

(2) Buqa, H.; Goers, D.; Holzapfel, M.; Spahr, M. E.; Novák, P. High Rate Capability of Graphite Negative Electrodes for Lithium-Ion Batteries. *J. Electrochem. Soc.* **2005**, *152*, A474.

(3) Obrovac, M. N.; Krause, L. J. Reversible Cycling of Crystalline Silicon Powder. *J. Electrochem. Soc.* **2007**, *154*, A103.

(4) Cui, L.-F.; Ruffo, R.; Chan, C. K.; Peng, H.; Cui, Y. Crystalline-Amorphous Core−Shell Silicon Nanowires for High Capacity and High Current Battery Electrodes. *Nano Lett.* **2009**, *9*, 491−495.

(5) Liu, N.; Lu, Z.; Zhao, J.; McDowell, M. T.; Lee, H.-W.; Zhao, W.; Cui, Y. A Pomegranate-Inspired Nanoscale Design for Large-Volume-Change Lithium Battery Anodes. *Nat. Nanotechnol.* **2014**, *9*, 187−192.

(6) Teki, R.; Datta, M. K.; Krishnan, R.; Parker, T. C.; Lu, T.-M.; Kumta, P. N.; Koratkar, N. Nanostructured Silicon Anodes for Lithium Ion Rechargeable Batteries. *Small* **2009**, *5*, 2236−2242.

(7) Saint, J.; Morcrette, M.; Larcher, D.; Laffont, L.; Beattie, S.; Pérès, J.-P.; Talaga, D.; Couzi, M.; Tarascon, J.-M. Towards a Fundamental Understanding of the Improved Electrochemical Performance of Silicon−Carbon Composites. *Adv. Funct. Mater.* **2007**, *17*, 1765−1774.

(8) Bogart, T. D.; Oka, D.; Lu, X.; Gu, M.; Wang, C.; Korgel, B. A. Lithium Ion Battery Peformance of Silicon Nanowires with Carbon Skin. *ACS Nano* **2014**, *8*, 915−922.

(9) Haridas, A. K.; Nguyen, Q. A.; Song, B. F.; Blaser, R.; Biswal, S. L. ALD-Modified LiNi0.33Mn0.33Co0.33O2 Paired with Macroporous Silicon for Lithium-Ion Batteries: An Investigation on Lithium Trapping, Resistance Rise, and Cycle-Life Performance. *ACS Appl. Energy Mater.* **2020**, *3*, 456−468.

(10) Song, B. F.; Dhanabalan, A.; Biswal, S. L. Evaluating the Capacity Ratio and Prelithiation Strategies for Extending Cyclability in Porous Silicon Composite Anodes and Lithium Iron Phosphate Cathodes for High Capacity Lithium-Ion Batteries. *J. Energy Storage* **2020**, *28*, 101268.

(11) Thakur, M.; Isaacson, M.; Sinsabaugh, S. L.; Wong, M. S.; Biswal, S. L. Gold-Coated Porous Silicon Films as Anodes for Lithium Ion Batteries. *J. Power Sources* **2012**, *205*, 426−432.

(12) Wu, H.; Cui, Y. Designing Nanostructured Si Anodes for High Energy Lithium Ion Batteries. *Nano Today* **2012**, *7*, 414−429.

(13) Ge, M.; Rong, J.; Fang, X.; Zhou, C. Porous Doped Silicon Nanowires for Lithium Ion Battery Anode with Long Cycle Life. *Nano Lett.* **2012**, *12*, 2318−2323.

(14) Yao, Y.; McDowell, M. T.; Ryu, I.; Wu, H.; Liu, N.; Hu, L.; Nix, W. D.; Cui, Y. Interconnected Silicon Hollow Nanospheres for Lithium-Ion Battery Anodes with Long Cycle Life. *Nano Lett.* **2011**, *11*, 2949−2954.

(15) Su, X.; Wu, Q.; Li, J.; Xiao, X.; Lott, A.; Lu, W.; Sheldon, B. W.; Wu, J. Silicon-Based Nanomaterials for Lithium-Ion Batteries: A Review. *Adv. Energy Mater.* **2014**, *4*, 1300882.

(16) Thakur, M.; Sinsabaugh, S. L.; Isaacson, M. J.; Wong, M. S.; Biswal, S. L. Inexpensive Method for Producing Macroporous Silicon Particulates (MPSPs) with Pyrolyzed Polyacrylonitrile for Lithium Ion Batteries. *Sci. Rep.* **2012**, *2*, 795.

(17) Li, Z.-F.; Zhang, H.; Liu, Q.; Liu, Y.; Stanciu, L.; Xie, J. Novel Pyrolyzed Polyaniline-Grafted Silicon Nanoparticles Encapsulated in Graphene Sheets As Li-Ion Battery Anodes. *ACS Appl. Mater. Interfaces* **2014**, *6*, 5996−6002.

(18) Li, J.; Lewis, R. B.; Dahn, J. R. Sodium Carboxymethyl Cellulose: A Potential Binder for Si Negative Electrodes for Li-Ion Batteries. *Electrochem. Solid-State Lett.* **2006**, *10*, A17.

(19) Li, J.; Le, D.-B.; Ferguson, P. P.; Dahn, J. R. Lithium Polyacrylate as a Binder for Tin−Cobalt−Carbon Negative Electrodes in Lithium-Ion Batteries. *Electrochim. Acta* **2010**, *55*, 2991−2995.

(20) Kovalenko, I.; Zdyrko, B.; Magasinski, A.; Hertzberg, B.; Milicev, Z.; Burtovyy, R.; Luzinov, I.; Yushin, G. A Major Constituent of Brown Algae for Use in High-Capacity Li-Ion Batteries. *Science* **2011**, *334*, 75−79.

(21) Wu, H.; Yu, G.; Pan, L.; Liu, N.; McDowell, M. T.; Bao, Z.; Cui, Y. Stable Li-Ion Battery Anodes by in-Situ Polymerization of Conducting Hydrogel to Conformally Coat Silicon Nanoparticles. *Nat. Commun.* **2013**, *4*, 1943.

(22) Shi, Y.; Zhou, X.; Yu, G. Material and Structural Design of Novel Binder Systems for High-Energy, High-Power Lithium-Ion Batteries. *Acc. Chem. Res.* **2017**, *50*, 2642−2652.

(23) Miranda, A.; Sarang, K.; Gendensuren, B.; Oh, E.-S.; Lutkenhaus, J.; Verduzco, R. Molecular Design Principles for Polymeric Binders in Silicon Anodes. *Mol. Syst. Des. Eng.* **2020**, *5*, 709−724.

(24) Lopez, J.; Mackanic, D. G.; Cui, Y.; Bao, Z. Designing Polymers for Advanced Battery Chemistries. *Nat. Rev. Mater.* **2019**, *4*, 312−330.

(25) Nguyen, V. A.; Kuss, C. Review—Conducting Polymer-Based Binders for Lithium-Ion Batteries and Beyond. *J. Electrochem. Soc.* **2020**, *167*, No. 065501.

(26) Zhao, Y.-M.; Yue, F.-S.; Li, S.-C.; Zhang, Y.; Tian, Z.-R.; Xu, Q.; Xin, S.; Guo, Y.-G. Advances of Polymer Binders for Silicon-Based Anodes in High Energy Density Lithium-Ion Batteries. *InfoMat* **2021**, *3*, 460−501.

(27) Thakur, M.; Pernites, R. B.; Nitta, N.; Isaacson, M.; Sinsabaugh, S. L.; Wong, M. S.; Biswal, S. L. Freestanding Macroporous Silicon and Pyrolyzed Polyacrylonitrile As a Composite Anode for Lithium Ion Batteries. *Chem. Mater.* **2012**, *24*, 2998−3003.

(28) Piper, D. M.; Yersak, T. A.; Son, S.-B.; Kim, S. C.; Kang, C. S.; Oh, K. H.; Ban, C.; Dillon, A. C.; Lee, S.-H. Conformal Coatings of Cyclized-PAN for Mechanically Resilient Si Nano-Composite Anodes. *Adv. Energy Mater.* **2013**, *3*, 697−702.

(29) Shen, L.; Shen, L.; Wang, Z.; Chen, L. In Situ Thermally Cross-Linked Polyacrylonitrile as Binder for High-Performance Silicon as Lithium Ion Battery Anode. *ChemSusChem* **2014**, *7*, 1951−1956.

(30) Luo, L.; Xu, Y.; Zhang, H.; Han, X.; Dong, H.; Xu, X.; Chen, C.; Zhang, Y.; Lin, J. Comprehensive Understanding of High Polar

Polyacrylonitrile as an Effective Binder for Li-Ion Battery Nano-Si Anodes. *ACS Appl. Mater. Interfaces* **2016**, *8*, 8154−8161.
(31) Gong, L.; Nguyen, M. H. T.; Oh, E.-S. High Polar Polyacrylonitrile as a Potential Binder for Negative Electrodes in Lithium Ion Batteries. *Electrochem. Commun.* **2013**, *29*, 45−47.
(32) Wang, X.; Zhang, Y.; Shi, Y.; Zeng, X.; Tang, R.; Wei, L. Conducting Polyaniline/Poly (Acrylic Acid)/Phytic Acid Multifunctional Binders for Si Anodes in Lithium Ion Batteries. *Ionics* **2019**, *25*, 5323−5331.
(33) McDowell, M. T.; Lee, S. W.; Nix, W. D.; Cui, Y. 25th Anniversary Article: Understanding the Lithiation of Silicon and Other Alloying Anodes for Lithium-Ion Batteries. *Adv. Mater.* **2013**, *25*, 4966−4985.
(34) Sandu, G.; Brassart, L.; Gohy, J.-F.; Pardoen, T.; Melinte, S.; Vlad, A. Surface Coating Mediated Swelling and Fracture of Silicon Nanowires during Lithiation. *ACS Nano* **2014**, *8*, 9427−9436.
(35) Luo, L.; Yang, H.; Yan, P.; Travis, J. J.; Lee, Y.; Liu, N.; Molina Piper, D.; Lee, S.-H.; Zhao, P.; George, S. M.; Zhang, J.-G.; Cui, Y.; Zhang, S.; Ban, C.; Wang, C.-M. Surface-Coating Regulated Lithiation Kinetics and Degradation in Silicon Nanowires for Lithium Ion Battery. *ACS Nano* **2015**, *9*, 5559−5566.
(36) Li, P.; Chen, G.; Zhang, N.; Ma, R.; Liu, X. β-Cyclodextrin as Lithium-Ion Diffusion Channel with Enhanced Kinetics for Stable Silicon Anode. *Energy Environ. Mater.* **2021**, *4*, 72−80.
(37) Liu, G.; Xun, S.; Vukmirovic, N.; Song, X.; Olalde-Velasco, P.; Zheng, H.; Battaglia, V. S.; Wang, L.; Yang, W. Polymers with Tailored Electronic Structure for High Capacity Lithium Battery Electrodes. *Adv. Mater.* **2011**, *23*, 4679−4683.
(38) Wu, M.; Xiao, X.; Vukmirovic, N.; Xun, S.; Das, P. K.; Song, X.; Olalde-Velasco, P.; Wang, D.; Weber, A. Z.; Wang, L.-W.; Battaglia, V. S.; Yang, W.; Liu, G. Toward an Ideal Polymer Binder Design for High-Capacity Battery Anodes. *J. Am. Chem. Soc.* **2013**, *135*, 12048−12056.
(39) Raju, M.; Ganesh, P.; Kent, P. R. C.; van Duin, A. C. T. Reactive Force Field Study of Li/C Systems for Electrical Energy Storage. *J. Chem. Theory Comput.* **2015**, *11*, 2156−2166.
(40) Jung, H.; Lee, M.; Yeo, B. C.; Lee, K.-R.; Han, S. S. Atomistic Observation of the Lithiation and Delithiation Behaviors of Silicon Nanowires Using Reactive Molecular Dynamics Simulations. *J. Phys. Chem. C* **2015**, *119*, 3447−3455.
(41) Ostadhossein, A.; Kim, S.-Y.; Cubuk, E. D.; Qi, Y.; van Duin, A. C. T. Atomic Insight into the Lithium Storage and Diffusion Mechanism of SiO2/Al2O3 Electrodes of Lithium Ion Batteries: ReaxFF Reactive Force Field Modeling. *J. Phys. Chem. A* **2016**, *120*, 2114−2127.
(42) Saha, B.; Schatz, G. C. Carbonization in Polyacrylonitrile (PAN) Based Carbon Fibers Studied by ReaxFF Molecular Dynamics Simulations. *J. Phys. Chem. B* **2012**, *116*, 4684−4692.
(43) Saha, B.; Furmanchuk, A.; Dzenis, Y.; Schatz, G. C. Multi-Step Mechanism of Carbonization in Templated Polyacrylonitrile Derived Fibers: ReaxFF Model Uncovers Origins of Graphite Alignment. *Carbon* **2015**, *94*, 694−704.
(44) Vashisth, A.; Ashraf, C.; Zhang, W.; Bakis, C. E.; van Duin, A. C. T. Accelerated ReaxFF Simulations for Describing the Reactive Cross-Linking of Polymers. *J. Phys. Chem. A* **2018**, *122*, 6633−6642.
(45) Min, K.; Kim, Y.; Goyal, S.; Lee, S. H.; McKenzie, M.; Park, H.; Savoy, E. S.; Rammohan, A. R.; Mauro, J. C.; Kim, H.; Chae, K.; Lee, H. S.; Shin, J.; Cho, E. Interfacial Adhesion Behavior of Polyimides on Silica Glass: A Molecular Dynamics Study. *Polymer* **2016**, *98*, 1−10.
(46) Min, K.; Rammohan, A. R.; Lee, H. S.; Shin, J.; Lee, S. H.; Goyal, S.; Park, H.; Mauro, J. C.; Stewart, R.; Botu, V.; Kim, H.; Cho, E. Computational Approaches for Investigating Interfacial Adhesion Phenomena of Polyimide on Silica Glass. *Sci. Rep.* **2017**, *7*, 10475.
(47) Kim, S.-P.; van Duin, A. C. T.; Shenoy, V. B. Effect of Electrolytes on the Structure and Evolution of the Solid Electrolyte Interphase (SEI) in Li-Ion Batteries: A Molecular Dynamics Study. *J. Power Sources* **2011**, *196*, 8590−8597.
(48) Bhati, M.; Senftle, T. P. Identifying Adhesion Properties at Si/Polymer Interfaces with ReaxFF. *J. Phys. Chem. C* **2019**, 27036.
(49) Teoh, H.; Metz, P. D.; Wilhelm, W. G. Electrical Conductivity of Pyrolyzed Polyacrylonitrile. *Mol. Cryst. Liq. Cryst.* **1982**, *83*, 297−306.
(50) Bruck, S. D. SEMICONDUCTING AND CONDUCTING ORGANIC PYROPOLYMERS. *Ind. Eng. Chem.* **1967**, *59*, 18−28.
(51) Renschler, C. L.; Sylwester, A. P. Conductive, Spin-cast Carbon Films from Polyacrylonitrile. *Appl. Phys. Lett.* **1987**, *50*, 1420−1422.
(52) Pan, L.; Yu, G.; Zhai, D.; Lee, H. R.; Zhao, W.; Liu, N.; Wang, H.; Tee, B. C.-K.; Shi, Y.; Cui, Y.; Bao, Z. Hierarchical Nanostructured Conducting Polymer Hydrogel with High Electrochemical Activity. *Proc. Natl. Acad. Sci.* **2012**, *109*, 9287−9292.
(53) Stejskal, J.; Riede, A.; Hlavatá, D.; Prokeš, J.; Helmstedt, M.; Holler, P. The Effect of Polymerization Temperature on Molecular Weight, Crystallinity, and Electrical Conductivity of Polyaniline. *Synth. Met.* **1998**, *96*, 55−61.
(54) Stejskal, J.; Gilbert, R. G. Polyaniline. Preparation of a Conducting Polymer(IUPAC Technical Report). *Pure Appl. Chem.* **2002**, *74*, 857−867.
(55) Chen, Y. A Review of Polyaniline Based Materials as Anodes for Lithiumion Batteries. *IOP Conf. Ser.: Mater. Sci. Eng.* **2019**, *677*, No. 022115.
(56) Islam, S.; Lakshmi, G. B. V. S.; Siddiqui, A. M.; Husain, M.; Zulfequar, M. Synthesis, Electrical Conductivity, and Dielectric Behavior of Polyaniline/V2O5 Composites. *Int. J. Polym. Sci.* **2013**, *2013*, No. e307525.
(57) Blinova, N. V.; Stejskal, J.; Trchová, M.; Prokeš, J.; Omastová, M. Polyaniline and Polypyrrole: A Comparative Study of the Preparation. *Eur. Polym. J.* **2007**, *43*, 2331−2341.
(58) Plimpton, S. Fast Parallel Algorithms for Short-Range Molecular Dynamics. *J. Comput. Phys.* **1995**, *117*, 1−19.
(59) Evans, D. J.; Holian, B. L. The Nose−Hoover Thermostat. *J. Chem. Phys.* **1985**, *83*, 4069−4074.
(60) Rahaman, M. S. A.; Ismail, A. F.; Mustafa, A. A Review of Heat Treatment on Polyacrylonitrile Fiber. *Polym. Degrad. Stab.* **2007**, *92*, 1421−1432.
(61) Xue, T. J.; McKinney, M. A.; Wilkie, C. A. The Thermal Degradation of Polyacrylonitrile. *Polym. Degrad. Stab.* **1997**, *58*, 193−202.
(62) Sanches, E. A.; da Silva, J. M. S.; Joelma, M. D. O.; Soares, J. C.; dos Santos, A. L.; Trovati, G.; Fernandes, E. G. R.; Mascarenhas, Y. P. Nanostructured Polyaniline Emeraldine-Base Form (EB-PANI): A Structural Investigation for Different Neutralization Times. *J. Mol. Struct.* **2014**, *1074*, 732−737.
(63) Mallikarjunachari, G.; Ghosh, P. Analysis of Strength and Response of Polymer Nano Thin Film Interfaces Applying Nanoindentation and Nanoscratch Techniques. *Polymer* **2016**, *90*, 53−66.
(64) Chen, L. B.; Xie, J. Y.; Yu, H. C.; Wang, T. H. An Amorphous Si Thin Film Anode with High Capacity and Long Cycling Life for Lithium Ion Batteries. *J. Appl. Electrochem.* **2009**, *39*, 1157−1162.
(65) Ding, N.; Xu, J.; Yao, Y. X.; Wegner, G.; Fang, X.; Chen, C. H.; Lieberwirth, I. Determination of the Diffusion Coefficient of Lithium Ions in Nano-Si. *Solid State Ionics* **2009**, *180*, 222−225.
(66) Ko, T.-H. The Influence of Pyrolysis on Physical Properties and Microstructure of Modified PAN Fibers during Carbonization. *J. Appl. Polym. Sci.* **1991**, *43*, 589−600.
(67) Gupta, N.; Rai, R.; Sikder, A.; Nandi, S.; Tanwar, A.; Khatokar, R.; Pask, S. D.; Mitra, S. Design and Development of a Poly-(Acrylonitrile-Co-Methyl Methacrylate) Copolymer to Improve the Viscoelastic and Surface Properties Critical to Scratch Resistance. *RSC Adv.* **2016**, *6*, 37933−37937.
(68) Valentová, H.; Stejskal, J. Mechanical Properties of Polyaniline. *Synth. Met.* **2010**, *160*, 832−834.

https://doi.org/10.1021/acsami.1c08484
ACS Appl. Mater. Interfaces 2021, 13, 41956−41967